Shap. Mem. Superelasticity
https://doi.org/10.1007/s40830-019-00230-9

TECHNICAL ARTICLE

FeMnNiAl Iron-Based Shape Memory Alloy: Promises and Challenges

W. Abuzaid[1] · Y. Wu[2] · R. Sidharth[2] · F. Brenne[2] · S. Alkan[2,3] · M. Vollmer[4] · P. Krooß[4] · T. Niendorf[4] · H. Sehitoglu[2]

Abstract Among all shape memory alloys, the iron-based FeMnNiAl has emerged as one of the most promising compositions with a huge superelasticity temperature window (> 400 °C). In this article, we first point to the high local transformation strains (> 10%) and high transformation stress levels (500–700 MPa) that result in a large work output. When subjected to either tensile or compressive loading, the transformation stress exhibits very small temperature dependence (Clausius–Clapeyron slope less than 0.2 MPa/°C in compression and 0.5 MPa/°C in tension) and an extremely small adiabatic temperature rise (less than 1 °C) during transformation. The complexity in transformation behavior associated with the presence of grain boundaries (GBs) is discussed. In particular, the work provides insight in the localization occurring at GBs due to transformation front–GB interactions and the potential cracking that can degrade fatigue performance. Overall, this work provides a deeper insight into the deformation response, advantages, and drawbacks of FeMnNiAl SMA. The comprehensive handling of various aspects of this alloy system paves the way for the development of future iron-based shape memory alloys.

Keywords FeMnNiAl · Superelasticity · Grain boundary · Functional fatigue · Elastocaloric effect

Introduction

The research efforts on iron-based shape memory alloys (Fe-SMAs) have produced intriguing results which motivate further studies in this field. Various alloy compositions have been investigated over the years providing insight into the properties, advantages, and some of the limitations of the developed Fe-SMAs. The early Fe-SMA research has been published by Hornbogen (Germany) [1], Koval (Ukraine) [2], Maki (Japan) [3], Sehitoglu (USA) [4–8], Chumlyakov (Russia) [9, 10] and more recently by Kainuma (Japan) [11, 12]. In general, the available Fe-based SMAs compositions have multiple elements including Mn, Co, Ni, and Ti which can be used to modify transformation temperatures, flow stresses, and transformation strains. In addition, the incorporation of aluminum, and the follow-up heat treatments create coherent precipitates which are responsible for superelasticity (SE). The precipitates do not transform but generate internal stress fields that assist with transformation [13]. In addition, the nano-scale precipitates act to increase the slip resistance which is conducive to martensitic transformation and SE. Previous efforts have highlighted two major concern areas curtailing SE in Fe-SMA; the difficulties in achieving reversible SE

Electronic supplementary material The online version of this article (https://doi.org/10.1007/s40830-019-00230-9) contains supplementary material, which is available to authorized users.

✉ W. Abuzaid
wabuzaid@aus.edu

✉ H. Sehitoglu
huseyin@illinois.edu

[1] Department of Mechanical Engineering, American University of Sharjah, PO Box 26666, Sharjah, United Arab Emirates

[2] Department of Mechanical Science and Engineering, University of Illinois at Urbana-Champaign, 1206 W. Green St., Urbana, IL 61801, USA

[3] Department of Mechanical Engineering, Boğaziçi University, Bebek, 34342 Istanbul, Turkey

[4] Institut für Werkstofftechnik (Materials Engineering), Universität Kassel, 34125 Kassel, Germany

Published online: 26 August 2019

transformation, particularly at room temperature, and the degradation in shape memory properties under cyclic loading (i.e., functional fatigue). The recently developed FeMnNiAl Fe-SMA addresses one of the major limitations by exhibiting SE across a wide range of temperatures, including room temperature SE which is desirable for a variety of applications [11]. Therefore, building on this background on Fe-based SMAs, the discovery of FeMnNiAl is a novel advancement that is worthy of further consideration [14–16]. The level of interest in FeMnNiAl is expected to increase in the next 10 years because of the superb functionalities of this Fe-SMA.

Various Fe-based SMA compositions have been considered in previous investigations. Earlier efforts have focused on FeMnSi and FeNiCoTi [2–5, 17, 18] systems while more recent studies have investigated the FeNiCoAlX (X = Ti, Ta, or Nb) [19, 20] Fe-based SMAs. Unlike FeMnSi, which undergoes face-centered cubic to hexagonal closed-packed transformation [17, 18], the FeNiCoTi and FeNiCoAlX sets of alloys undergo bcc (body-centered cubic) to bct (body-centered tetragonal) transformation. In the case of FeMnSi and FeNiCoTi, shape memory effect has been reported but no SE. Alloying with Al, in the case of FeNiCoAlX system, results in the formation of coherent nano-scale precipitates that are conducive to SE. In compositions which incorporate Nb, superelasticity is limited to low temperatures (below 0 °C) while the FeNiCoAlTi [7] and FeNiCoAlTa [21] exhibit superelasticity at room temperature and above with SE strain levels near 7%, but show rapid cyclic degradation. On the other hand, the newly discovered FeMnNiAl alloys undergo bcc to fcc transformation [22] with high transformation strains (10%) exceeding the levels in FeNiCoTi [7] and FeMnSi (< 3%) compositions.

While many Fe-based alloys point to large shape memory strains (> 10%) based on lattice constant calculations, the experimental results fall far short of the theoretical levels (< 7%). Therefore, the FeMnNiAl with strains as high as 10% defies the experience with other Fe-based SMA alloys. This is possibly due to the higher plastic deformation resistance which permits higher transformation strains [22]. We will show that the FeMnNiAl exhibits an unusually wide SE window ranging from cryogenic temperatures all the way to 400 °C under both tension and compression. The temperature limits at the high-temperature end have not been established previously and will, therefore, be addressed in the current study. From a practical perspective, exhibiting SE across a wide range of temperatures, including elevated temperatures nearing 400 °C, is very advantageous. This unique attribute can potentially help the development of new applications without the complication of needing to tailor composition and/or heat treatment to achieve a certain window of SE for a particular application. The versatility in achieving superelastic properties in FeMnNiAl is further enhanced by the fact that the transformation stress for this alloy system exhibits weak temperature dependence compared to other SMAs. This further simplifies the processes of developing applications employing the superelastic properties of this Fe-based SMA.

To appreciate the efficacy of FeMnNiAl compared to other SMAs, we present Figs. 1, 2 and 3 below which focus on three key practical aspects; the temperature range for which SE can be obtained, transformation stress and strain levels, and fracture resistance. In Fig. 1, the SE windows of several prominent SMAs are shown. It is noted that the widely utilized and commercially available NiTi SMA has a SE window of less than 100 °C. Copper-based alloys can reach a window of 200 °C while NiTiHf has a SE capability confined to high temperatures and exhibit a small superelastic window which therefore limits its range of application. Remarkably, the FeMnNiAl exhibits one of the highest SE windows nearing 500 °C along with the high-temperature CoNiGa [23] and FeNiGa [24] SMAs.

A comparison focusing on the transformation stress levels versus transformation strain is shown in Fig. 2. Note that depending on the specific application, a high transformation stress may be desirable such as for load-bearing structural applications. A combination of high transformation stress and high transformation strain produces a large work output that can be beneficial (e.g., in damping applications). Among the SMAs reviewed in Fig. 2, the FeMnNiAl alloy exhibits both, a substantial transformation strain far exceeding the other Fe-based SMAs, and high levels of transformation stresses. In comparison, although the FeNiGa, Cu-based (e.g., CuZnAl SMA), and NiTi-based SMAs can have higher transformation strains, the transformation stresses are typically much lower than what has been reported for FeMnNiAl.

Figure 3 addresses the topic of fracture resistance which has been receiving increasing attention in SMA research. SMAs, in general, have notoriously low fracture resistance and suffer from low intrinsic toughness. This is documented in Fig. 3 for various SMA compositions. The elastic moduli information is also included in the figure which is an important consideration in structural stiffness (axial, bending, etc.) and in the development of elastic energy storage systems upon transformation. According to our recent study on FeMnNiAl, the elastic moduli can vary from 100 to 195 GPa and fracture toughness from 19 to 33 MPa $m^{0.5}$ depending on the crystal orientations. The FeMnNiAl SMA exhibits similar fracture toughness compared to NiTi, however the moduli (stiffness) range is considerably higher which improves the elastic strain energy storage capacity of this Fe-based SMA.

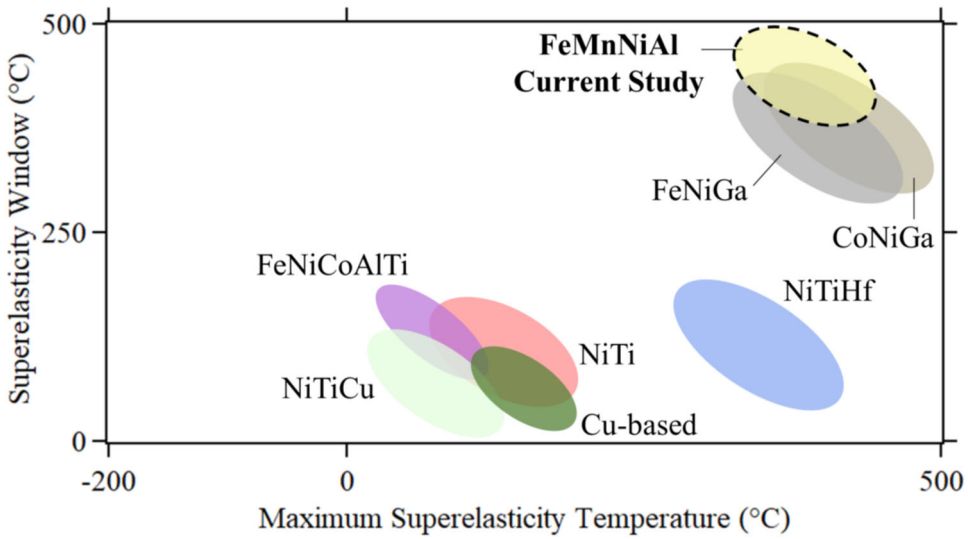

Fig. 1 The superelastic window versus the maximum SE temperature for various SMA systems. The FeMnNiAl Fe-based SMAs exhibit a remarkably wide superelastic window. The data represent the results of different compositions, heat treatments, tension/compression, poly-/single-crystalline, etc. (Color figure online)

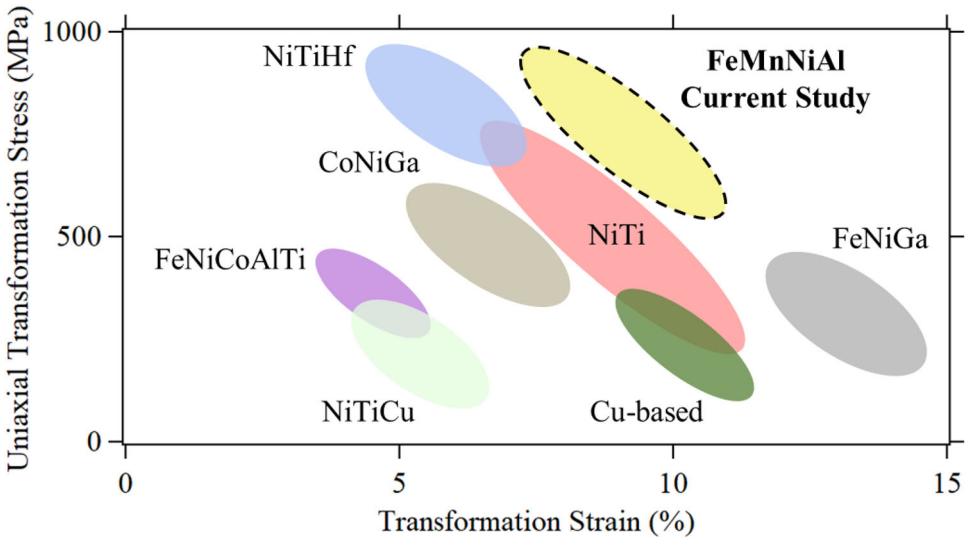

Fig. 2 Uniaxial transformation stress versus the transformation strain for various SMA systems. The results show that FeMnNiAl alloys exhibit remarkably favorable characteristics (Color figure online)

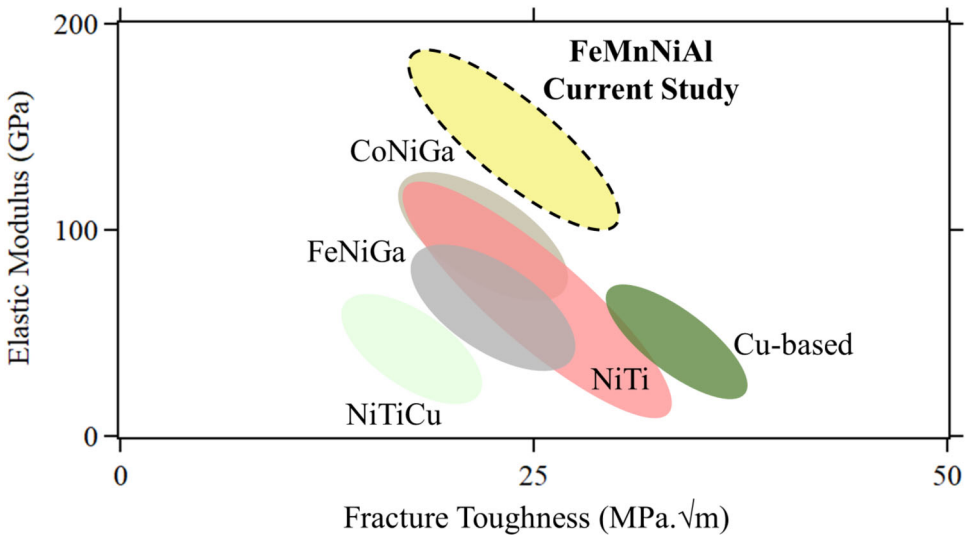

Fig. 3 Elastic modulus and fracture toughness plot for selected SMAs. The higher elastic moduli exhibited by FeMnNiAl can be advantageous in certain applications (Color figure online)

To establish the FeMnNiAl data presented in Figs. 1, 2 and 3, new experiments were conducted at various deformation temperatures and loading conditions. Specifically, while there is low-temperature data in the literature, the high temperature limit on SE required further investigation. The maximum transformation strain information at local scales in experiments was also not available. Local strain measurements permit to pinpoint exactly the transformation strain magnitudes.

Finally, we note that the adiabatic increase of temperature during repeated phase transformation (upon cycling) can develop due to latent heat [25]. In turn, the buildup of temperature has been linked to the nucleation of fatigue cracks in SMAs such as NiTi [25]. For the first time, we will discuss the limited temperature rise associated with the transformation in FeMnNiAl in comparison with other SMAs. This is a result of transformation with a small entropy change which is reflected through the rather small Clausius–Clapeyron slope as well. Such a small adiabatic temperature change has the potential to minimize the frequency effects in fatigue and strain rate sensitivity [26] that has hindered NiTi in certain applications.

Results

Superelasticity in Tension and Compression

In this study, both tension and compression behaviors of polycrystalline $Fe_{35}Mn_{34}Ni_{7.5}Al_{13.5}$ (at.%) samples were considered. The tensile specimens were machined using EDM into flat dog-bone geometries having 3×10 mm^2 gauge section and 1.5 mm thickness while the compression samples had 4×4 mm^2 cross section and a length of 8 mm. It should be noted that this Fe-based SMA does not perform well in the polycrystalline state because of propensity of fracture at grain boundaries and also the formation of a limited number of lattice correspondences. AGG heat treatment (abnormal grain growth treatment via thermal cycling), is typically required to promote grain growth and produce microstructures composed of bamboo type crystals, having diameters in the mm range, or single crystals. The AGG treatment involves cycling the temperature between 900 and 1225 °C multiple times followed by quenching into 80 °C warm water. Subsequently, an aging heat treatment (200–225 °C for 3–4 h) is required to introduce coherent nano-precipitates which are essential for thermoelastic martensitic transformation. Typical results are shown in Fig. 4 for tension. Digital image correlation (DIC) was used to monitor the accumulation of transformation strains and the subsequent recovery process during unloading. The full-field deformation maps allow for accurate assessment of the global (i.e., average response at the macroscale) as well as the localized behavior within the gauge section. The reported stress–strain curve shows room temperature SE with full strain recovery in the gauge section. The strain levels, at the macro-scale, reached about 10% global strain, while the local transformation magnitudes exceeded 12% as depicted from the strain contour plots shown as insets in Fig. 4a. The EBSD results obtained after AGG treatment and prior to loading are illustrated for this case (Fig. 4b, c) and point to predominately a single grain orientation in the gauge section. The grains marked as 1 and 3 in the EBSD map shown in Fig. 4b were mostly outside the gauge section of the dog-bone sample. Consequently, interfaces in the form of grain boundaries had negligible influence on the deformation response shown in Fig. 4a.

Figure 5 shows the results for a polycrystalline sample subjected to compression loading. The specimen was subjected to two loading increments at room temperature (25 °C); the first up to $\approx$ 3% global compression strain (black curve shown in Fig. 5a) and the second up to $\approx$ 5% global strain as reported with the red stress–strain curve in Fig. 5a. The stress–strain curves presented with dashed lines, as opposed to the solid lines used for the global response, were constructed using the localized strain region highlighted in the full-field strain contour plots shown in Fig. 5b. The local region represents a location on the sample's surface which experienced the largest amount of local transformation strain. The global strains are naturally less than these local strains due to lack of transformation in grains with unfavorable orientations or due to the transformation front being limited and not extending across the entire volume of transforming grains (i.e., partial transformation within grains). Grain boundaries can also influence and amplify the local strains due to incompatibilities across interfaces and/or the buildup of dislocation pileups and stress concentration at grain boundaries. These factors induce heterogeneities in the response leading to the dissimilar global and local transformation strains. In the case of FeMnNiAl SMA in particular, the grain size also impacts the attained levels of transformation strains as discussed previously in [27]. The EBSD grain orientation map and IPF (inverse-pole figure) for the compression sample are shown in Fig. 5c, d, respectively. Unlike the tensile sample discussed in Fig. 4, the AGG treatment did not result in the formation of a single crystal orientation in the gauge section of the compression sample. Therefore, the varying crystal orientations and the influence of grain boundaries in this case have resulted in a significant difference between the global and local transformation strains. It is worth noting, however, that there is a striking similarity between tension (Fig. 4) and compression (Fig. 5) global response for the room temperature deformation (i.e., notice the similarity in the critical transformation stresses

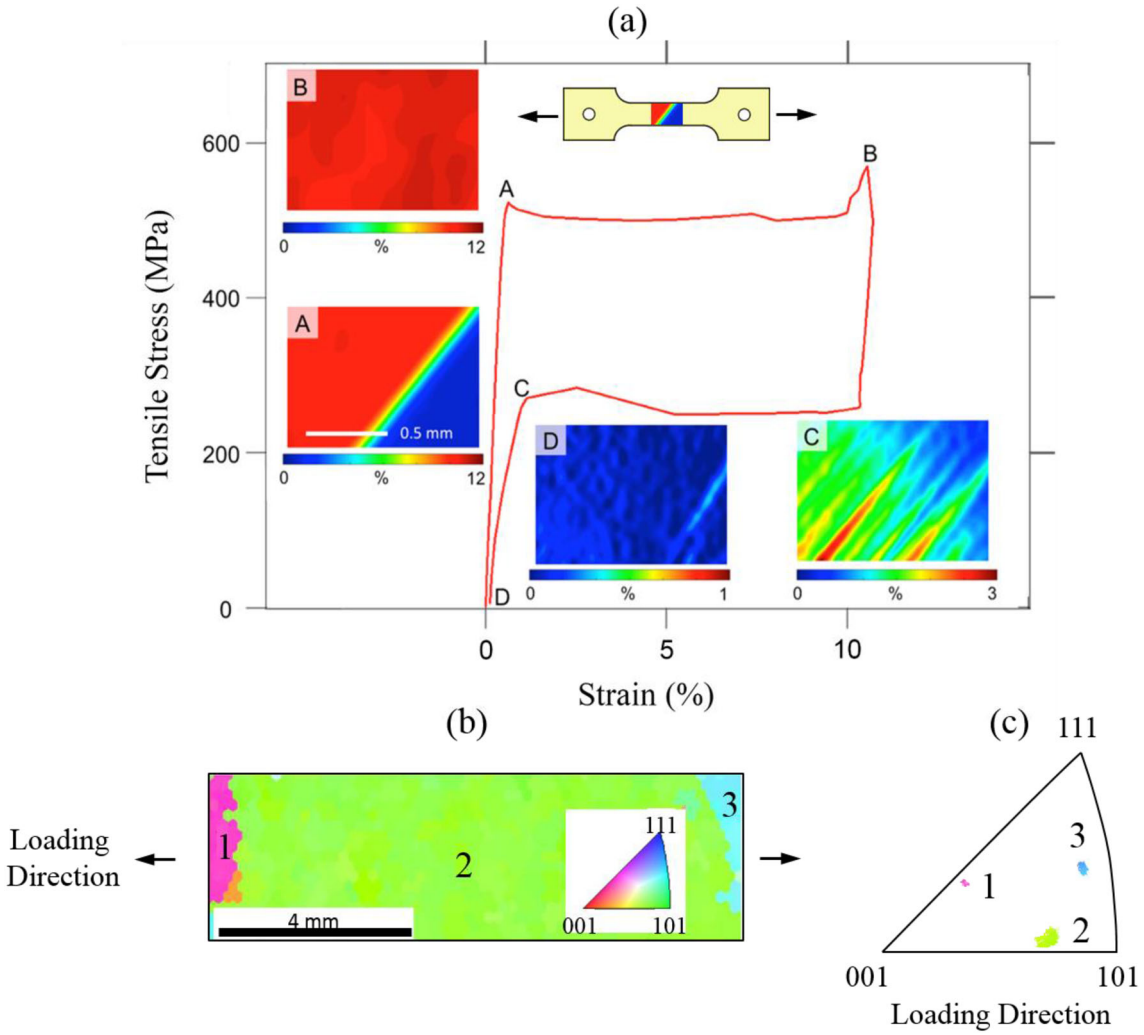

Fig. 4 **a** Stress–strain response at room temperature of FeMnNiAl subjected to tensile loading. The transformation front indicates strains exceeding 12%. **b** EBSD grain orientation map for the entire gauge section of the dogbone sample. **c** IPF highlighting the loading direction (Color figure online)

in both cases, tension and compression). This can be related to the microstructure, i.e., grain orientation.

The results reported in Figs. 4 and 5 highlight the room temperature response under both tensile and compressive loadings. One of the main advantages of FeMnNiAl SMA, however, has been the reported superelasticity over a wide range of temperatures extending from subzero (down to − 160 °C) to elevated temperatures (up to 240 °C) [11, 28]. In the current work, the superelastic response of FeMnNiAl was assessed over a wider range of temperatures, both in tension and compression loading. Figure 6a reports the global stress–strain curves for various specimens and loading temperatures (all in tension). Interestingly, clear superelasticity with full strain recovery was achieved even at 300 °C which is higher than what has been previously reported in the literature. It should be pointed out that some of the variation in the critical transformation stresses shown in Fig. 6a is attributed to the difference in crystal orientation and number of grains within the gauge sections of the investigated samples. For example, the results obtained at 100 and 200 °C deformation temperatures were collected from a specimen which developed primarily a single crystal orientation following the AGG heat treatment. The accumulation, and recovery, of transformation strains extended across the entire gauge section of the single crystal orientation as shown in the full-field contour plots in Fig. 6b. In the sample investigated at 300 and 400 °C, the AGG treatment did not result in a single crystalline gauge section but a bi-crystal with one of the grains having favorable orientation for reversible transformation. In this case, transformation commenced at a slightly lower stress, due to the different crystal orientation, and was localized and confined within one of the

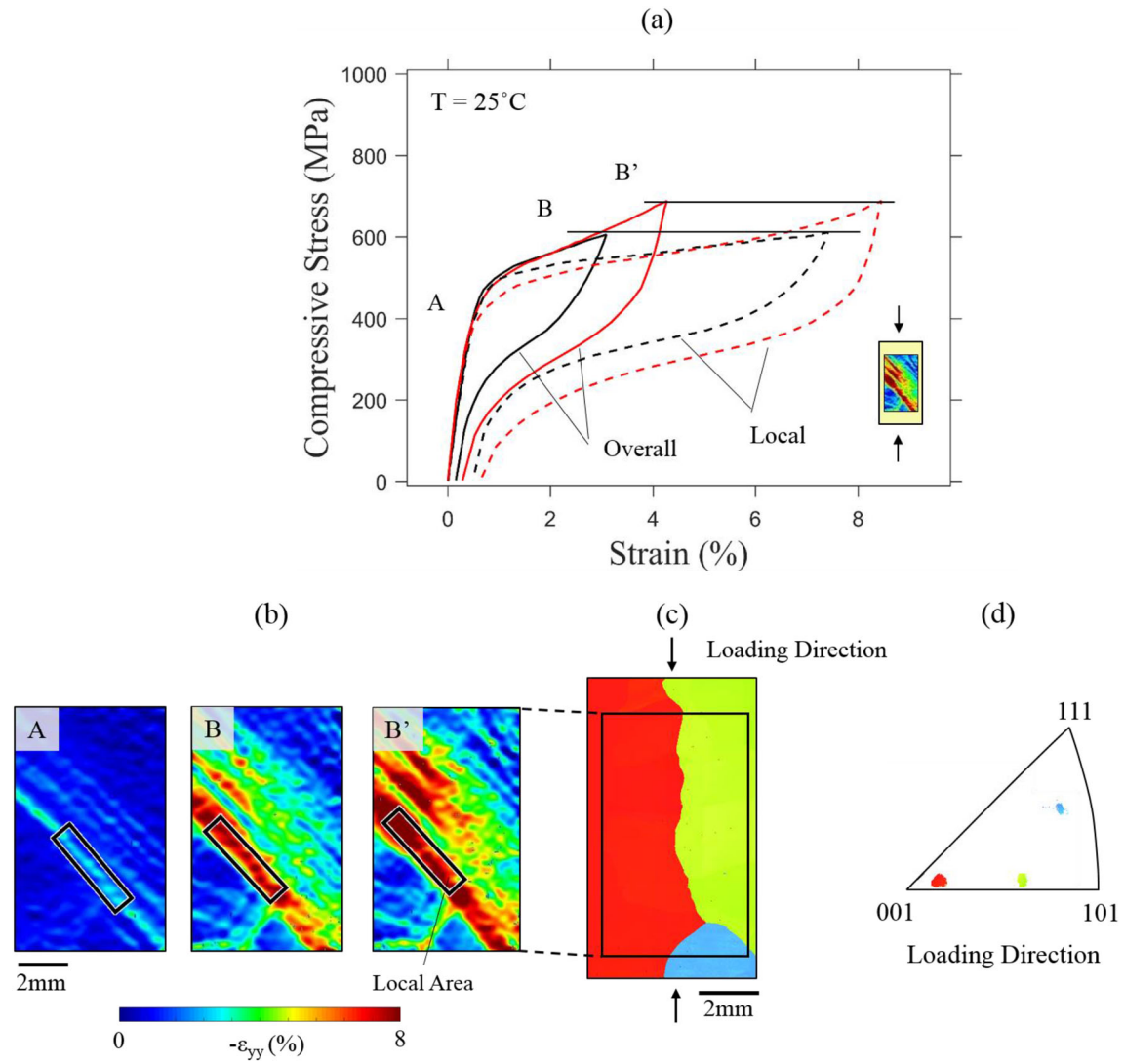

Fig. 5 **a** Stress–strain behavior of a polycrystalline sample subjected to compression. The local strain indicates levels exceeding 8% as shown in the full-field strain contour plots in **b**. The average strain across the entire gauge section was used to construct the overall stress–strain curve while the local represents the strain in the smaller region, marked in **b**, where transformation is localized. **c** EBSD grain orientation map for the entire gauge section and **d** the corresponding inverse-pole figure (Color figure online)

grains and did not extend across the entire gauge section as shown in Fig. 6c.

Permanent plastic deformation was observed at 400 °C deformation temperature. This was clearly measured from the global response (i.e., stress strain curve) and the local strain accumulation upon unloading as shown in the full-field strain contour plots in Fig. 6c. The local buildup of plastic strain took place in the same spatial location where reversible transformation took place at lower deformation temperatures (compare insets C' and D' in Fig. 6c). Although limited levels of residual strain took place at lower deformation temperatures, the gross accumulation of plastic strain at 400 °C deformation temperature, along with the absence of superelasticity, was potentially attributed to slip in the austenite phase.

In compression, superelasticity was also observed across a wide range of temperatures as shown in Fig. 7a. Full strain recovery was measured up to a remarkable 400 °C deformation temperature. The slope of the CC curve (Fig. 7b) was also very low indicating that the transformation stress is nearly constant over a broad temperature range (tension and compression). Eventually, plastic deformation commenced once the deformation temperature was raised to 450 °C. As visible by the DIC contour plot in Fig. 7e, the areas of increased strains resemble very well the direction of the martensite which formed at 300 °C. Thus, martensitic transformation still seems to be active. However, as reversed flow is not observed, plastic deformation due to slip and concomitant pinning of martensite dominates the unloading response. This could be confirmed

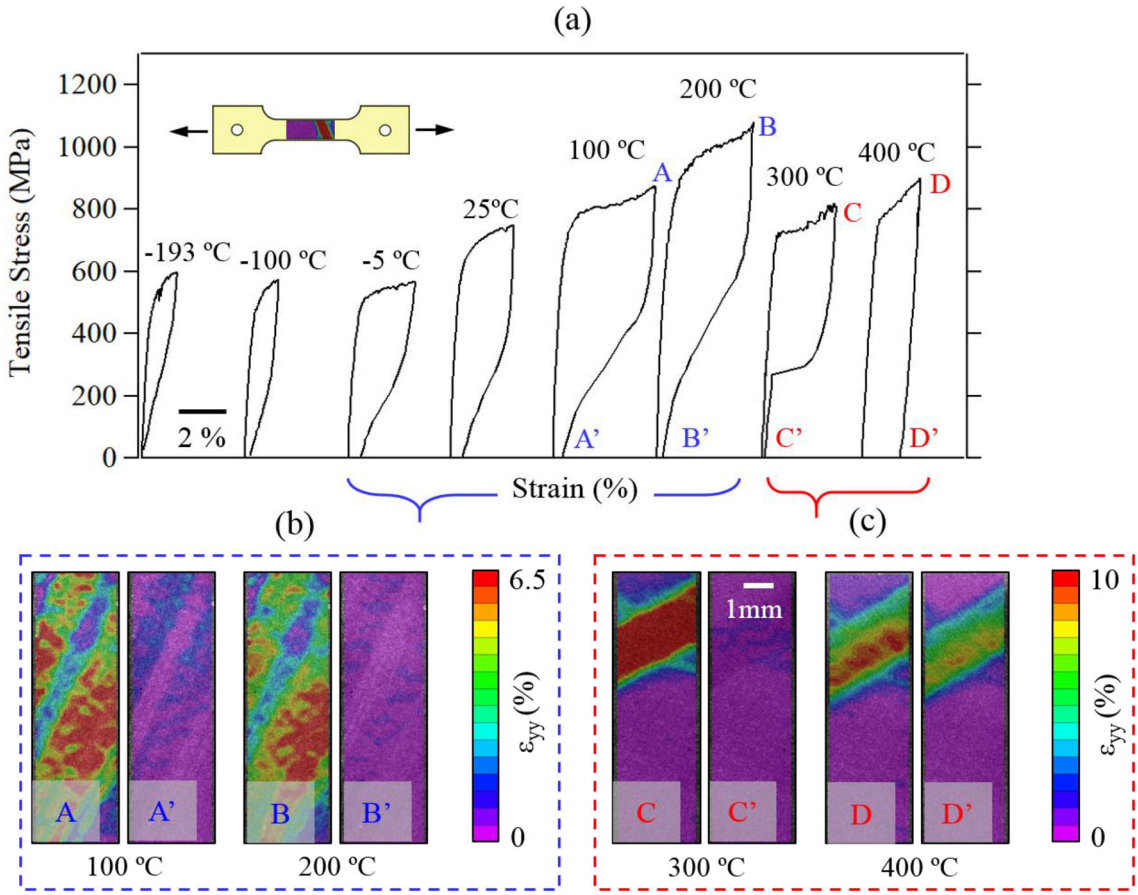

Fig. 6 **a** Stress–strain response of FeMnNiAl in tension at various deformation temperatures. **b** Full-field strain contour plots showing the strains at the maximum stress, and following unloading for the specimen deformed at 100 and 200 °C. **c** Full-field strain contour plots showing the strains at the maximum stress, and following unloading for the specimen deformed at 300 and 400 °C. Permanent accumulation of plastic strain is shown at 400 °C (Color figure online)

by TEM analysis at the end of the series of superelasticity experiments (50 °C to 400 °C) followed by apparent plastic behavior 450 °C (Fig. 8). Due to the loading history of the sample, accumulation of residual martensite, due to SE cycling at lower temperatures, and slip activity in the matrix at 450 °C are expected. The overview in Fig. 8a clearly shows the presence of retained martensite, which contributes to the remnant (plastic) deformation present after unloading at 450 °C (Fig. 7). The reason for the hindered recovery is rooted in increased dislocation activity, which for one thing additionally contributes to the remnant plastic deformation and for another thing pins the martensite. This phenomenon is elucidated in Fig. 8b showing slip bands and high dislocation density in the vicinity of the interface. Details of TEM specimen extraction are given in *Supplementary Material* section.

As discussed earlier, grain boundaries play a detrimental role in FeMnNiAl SMA superelastic response. Previous works have clearly highlighted limited levels of SE and the propensity to initiate fracture at grain boundaries in this alloy system. Figure 9 illustrates the superelastic response of another FeMnNiAl sample with a different, 'bamboo' structure compared to the one shown in Fig. 4b. The grain orientation and inverse-pole figure in the loading direction are showcased in Fig. 9c. The tensile sample was deformed monotonically at room temperature and the corresponding stress–strain curve is shown in Fig. 9a. The evolution of phase transformation is captured using DIC and 8 DIC snapshots are shown in Fig. 9b to elucidate the movement of the transformation front. The stress drops (Points B and C) during the loading process can be rationalized by either the nucleation of a new martensitic variant or the propagation of the transformation front as evident in Fig. 9b. It is also important to note that the transformation only takes place in the orange grain which is close to <103> loading orientation. This can be attributed to two mechanisms. Firstly, the orientation of <103> grain can be more favorable for phase transformation compared to other grains. Secondly, the grain boundary can serve as an obstacle for the migration of the transformation front.

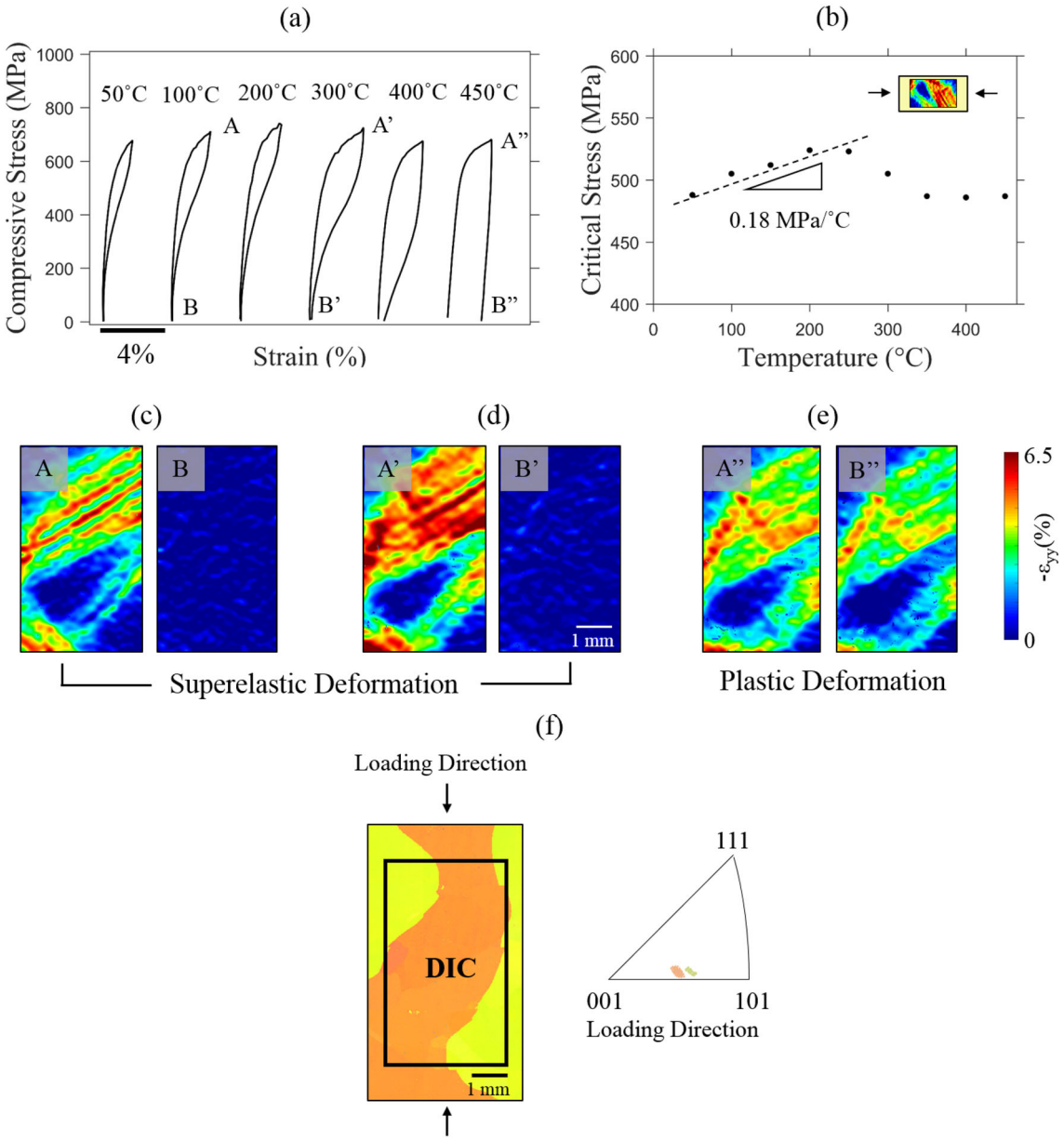

Fig. 7 **a** Stress–strain response of FeMnNiAl in compression at various deformation temperatures. **b** The Clausius–Clapeyron curve generated from the results reported in **a**. **c**–**e** Full-field strain contour plots showing the strains at the maximum stress, and following unloading for the specimen deformed at 100, 300, and 450 °C, respectively. **f** EBSD grain orientation map and the corresponding inverse-pole figure for the entire gauge section (Color figure online)

Cyclic Response and Functional Fatigue

One of the major shortcomings of FeMnNiAl, and Fe-based SMAs in general, relates to their functional fatigue performance when subjected to cyclic loading. An example for a tension sample subjected to 12 consecutive loading cycles, at room temperature, is shown in Fig. 10. The stress–strain curves (Fig. 10a) highlights clear accumulation of residual strains ($\varepsilon_{residual}$) with continued loading. The gauge section of the considered sample comprised two grains as shown in Fig. 10d. The optical images (Fig. 10b), which were obtained following complete unloading, visually point to local changes in Grain 2 due to the accumulation of residual strain. A quantitative summary of $\varepsilon_{residual}$ as a function of cycle number is presented in Fig. 10c. Initially and in the first few cycles, small residual strain levels were measured. However, the rate of $\varepsilon_{residual}$ buildup, and loss of functionality, accelerated significantly beyond the 5th loading cycle.

To further explore the complexities induced by GBs in fatigue, high-resolution DIC was utilized to investigate interactions in the vicinity of the GB for the fatigue sample

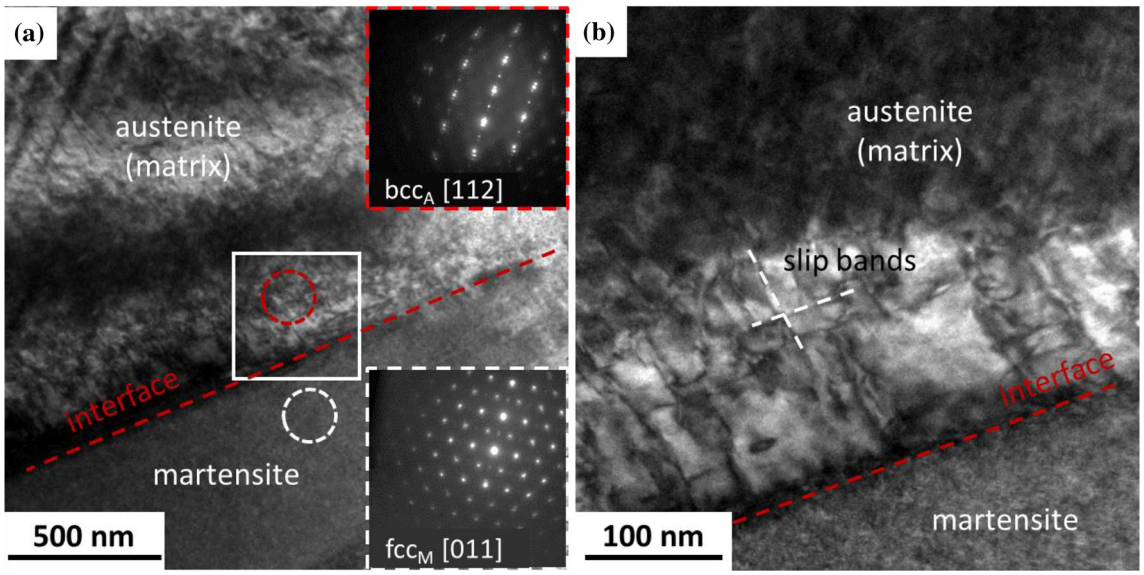

Fig. 8 **a** Bright-field TEM image after the compressive testing sequence shown in Fig. 7a. Until 450 °C the deformation is fully recovered. Finally, upon unloading at 450 °C there is strong evidence of retained martensite (lower area) in the austenitic matrix (upper area) and plastic flow (see also supplementary material). The corresponding SAED patterns recorded from the areas marked by the dashed white and red circles are given in the insets to the bottom and top, respectively. The area marked by the white square in **a** is given at higher magnification in **b**. Close to the interface, slip bands are perceptible indicating high dislocation activity and pinning of martensite at high load levels (Color figure online)

discussed in Fig. 10. The stress–strain curves shown in Fig. 11a represent the global (entire gauge section) and local behaviors (GB region as outlined in Fig. 11b) for the 12th loading cycle. Very high levels of local strains were measured at the interface. The representative strain contour plots of the local GB region are shown in Fig. 11c. Although the DIC data obtained at this level point to transformation taking place on both sides across the interface, earlier measurement cycles have revealed transformation to be confined in Grain 2 only. As the transformation front impinged on the GB (Fig. 11b), the accumulation of residual strains (dislocations) with continued loading altered the local stress levels in the vicinity of the GB. After the 10th loading cycle, transformation nucleating at the GB was observed in Grain 1. This nucleation was accompanied by very high levels of deformation at the interface as inferred by the contour plots showing localized strains in the GB region. The initiation of a fatigue micro-crack was eventually observed in this local region.

Elastocaloric Effect

Figure 12 demonstrates the superelasticity of a FeMiNiAl single crystal orientated near the <257> pole at 28.5 °C. The EBSD map and inverse-pole figure are shown in Fig. 12c to attest the grain orientation. In addition to strain measurement, the temperature change of the sample was also recorded during the loading and unloading cycles using an infrared camera. To prevent excessive self-heating during forward phase transformation (A to M), the loading process was performed using a small strain rate, 0.001 s^{-1}. However, the unloading was carried out with a large strain rate, 0.2 s^{-1}, to limit the heat exchange between the sample and its surroundings so that the intrinsic temperature change can be elicited. The thermographs taken by the infrared camera are presented in Fig. 12a along with the DIC strain contours at different load steps (shown as insets marked with IR and DIC). Note that the localizations on both DIC strain contours and thermographs correspond to each other very well. The evolution of temperature is illustrated in Fig. 12b for two consecutive cycles. It is evident that the temperature drops (ΔT) are 1.2 °C and 0.9 °C for cycle 1 and cycle 2, respectively, after rapid unloading. When compared to NiTi which exhibits ΔT on the order of 18.2 °C, those of FeMnNiAl alloys fall far short. The slightly lower temperature change in cycle 2 can be ascribed to the functional degradation of the alloys upon cycling (Fig. 10).

Discussion of Results

Advantages of FeMnNiAl SMAs

The clear benefits of FeMnNiAl alloys are the unprecedented window of superelasticity, the high transformation stresses, and the relatively small temperature rise during

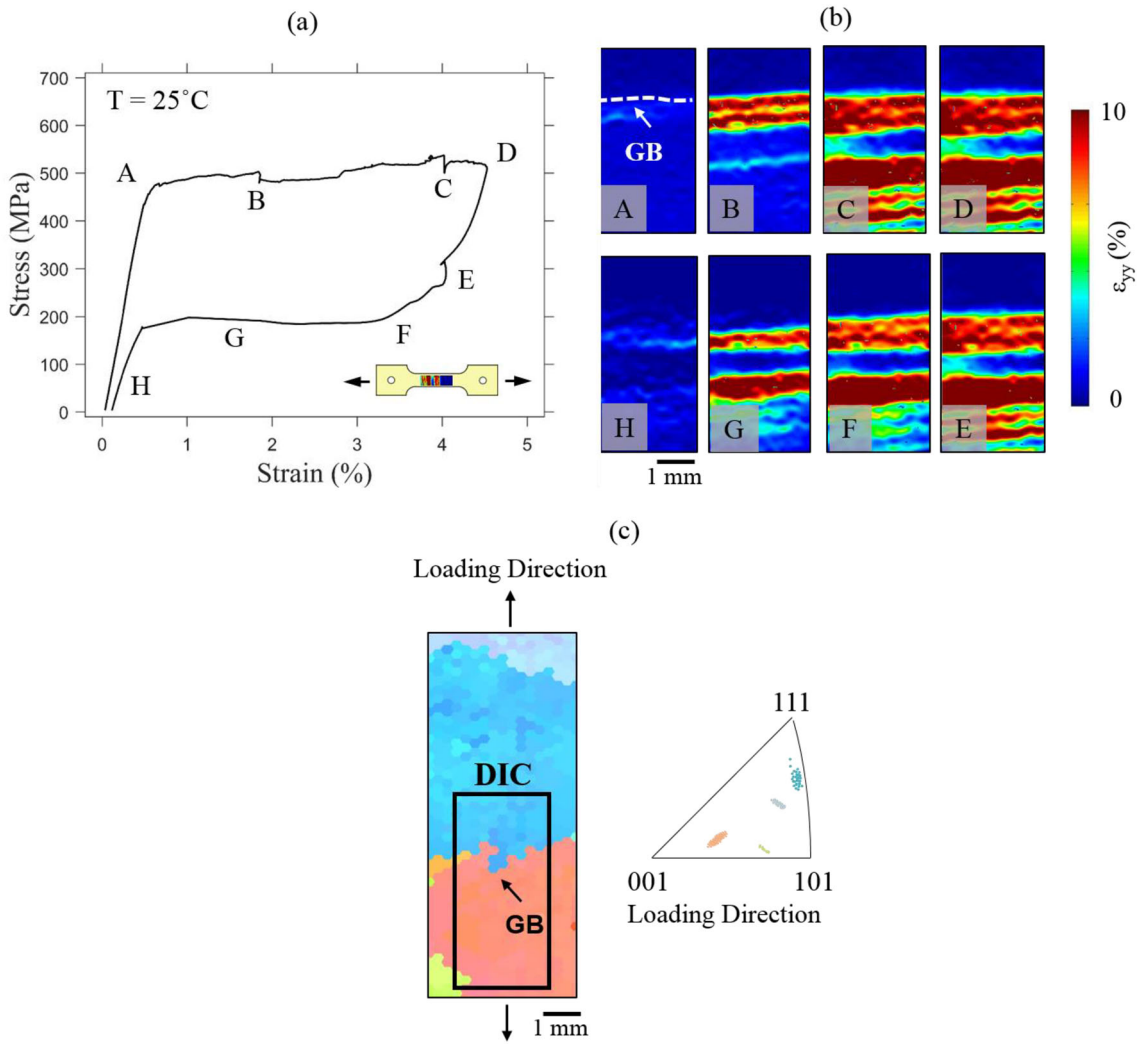

Fig. 9 **a** The superelastic response of FeMnNiAl SMAs at room temperature. **b** DIC strain contour plots at different load steps are shown to demonstrate the evolution of the transformation zone. Note that the transformation blockage at a grain boundary resulting in curtailing of transformation (see movie as the auxiliary file). **c** The EBSD map demonstrates the layout of the grains in the sample and the inverse-pole figure shows the grain orientation of each grain. The DIC region is marked on the EBSD map (Color figure online)

transformation. The ability to achieve superelastic response over such a large range of temperatures, with a single heat treatment, enables huge simplifications from a practical perspective. For example, NiTi SMA transformation temperatures can be adjusted and shifted to exhibit superelasticity or shape memory effect over a 100 °C temperature range. However, and unlike FeMnNiAl, the gap between the transformation temperatures is not as wide and custom heat treatments are therefore required for each set of conditions. FeMnNiAl only requires a single heat treatment to exhibit superelasticity over a 500 °C temperature range (− 193 to 300 °C as shown in this work). In addition, the relatively lower cost of FeMnNiAl compared to other SMA alloys and the high stiffness compared to NiTi and Cu-based SMAs can be exploited in certain applications requiring larger load carrying capacities and/or larger elastic strain energy storage capacity (e.g., for structural damping applications). In addition, although the focus in this paper and in the published literature has been on superelastic behavior, the FeMnNiAl SMA can exhibit shape memory response when subjected to certain aging treatments. With proper control, this Fe-based SMA can be tailored to show superelasticity, shape memory effect, or both upon unloading. The microstructural details responsible for this complex behavior has been virtually not investigated and left for future studies. Nevertheless, this property opens the room to adapt the alloy response to a wider range of applications.

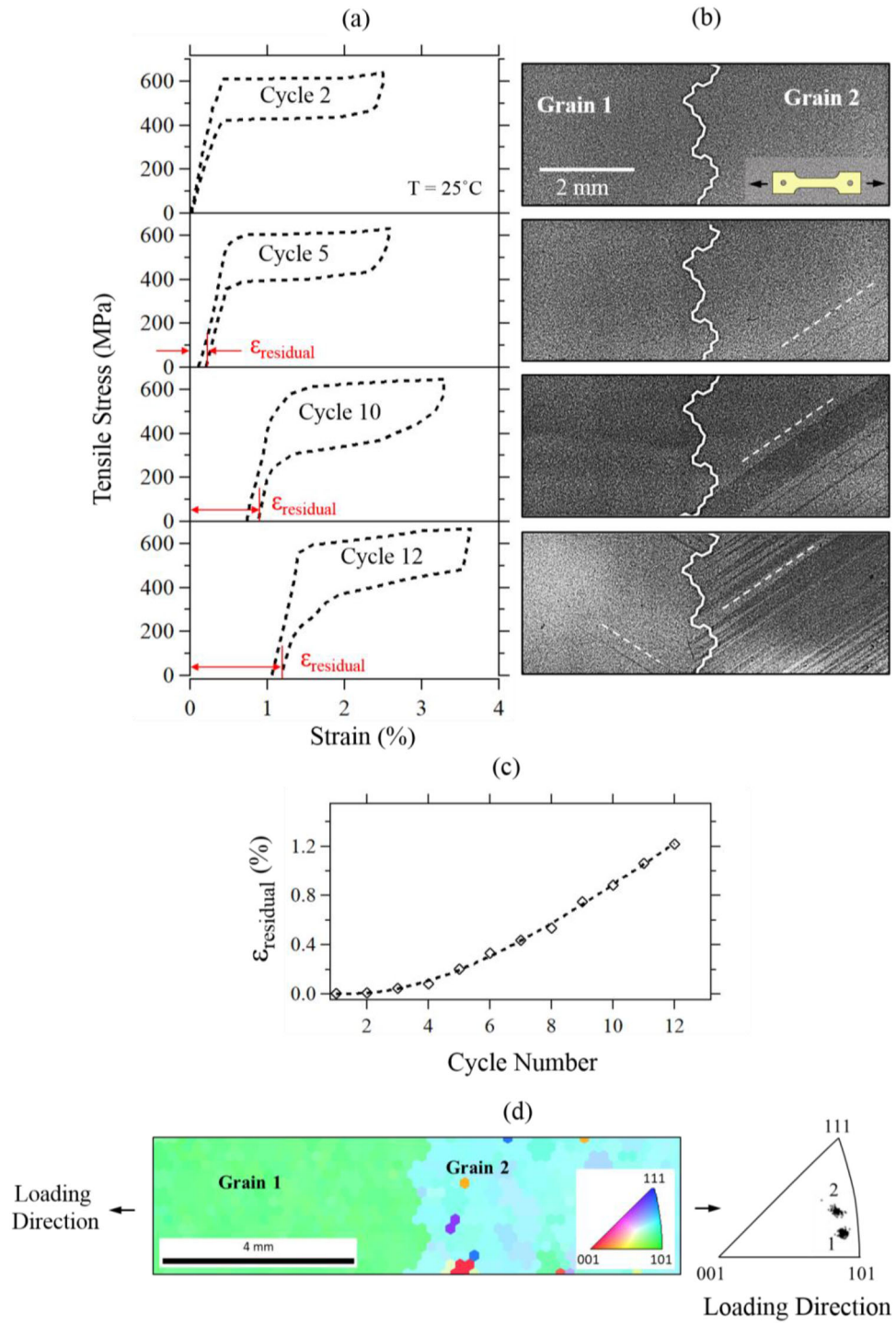

Fig. 10 **a** Stress–strain response of FeMnNiAl tension sample subjected to cyclic loading. **b** Optical images of the sample's surface at the end of selected fatigue cycles. Visual changes in Grain 2 relate to the accumulation of residual strains and loss of functionality. **c** Summary of the residual strain evolution with fatigue loading. **d** The EBSD grain orientation map and inverse-pole figure of the bi-crystalline material local region (Color figure online)

Challenges of FeMnNiAl SMAs

Despite the clear benefits of FeMnNiAl SMA, there remain significant challenges facing the community which prevent a wider adoption and hinder application development. The major challenges are primarily: (1) evidence of early fracture initiation especially at grain boundaries; (2) the development of plastic strain with cycling (under repeated transformations), and (3) the tremendous sensitivity of superelastic properties to aging treatments including the rate of cooling. If these issues are addressed then it would be possible to utilize these alloys in widespread applications. Among the listed challenges, the functional fatigue properties of FeMnNiAl Fe-based SMA is in fact one of the major limitations of this alloy. Compared to the NiTi or Cu-based SMAs, cyclic degradation of superelasticity

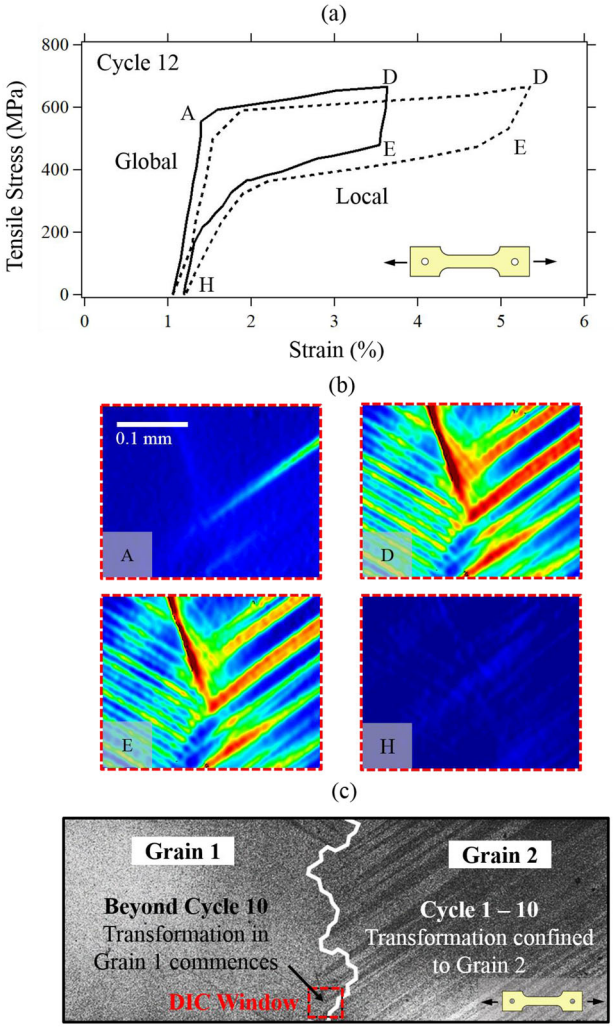

Fig. 11 **a** A representative global and local stress–strain response of FeMnNiAl tension sample subjected to cyclic loading. **b** Strain contour plots at different stress levels for the local region highlighted with a red box in **c**. **c** Optical image of the sample's surface showing signs of irrecoverable transformation in Grain 2 and the nucleation of new transformation in Grain 1 due to localization at the GB. The plots point to transformation in both grains and high levels of strain localization at the interface (Color figure online)

occurs rapidly resulting in complete loss of functionality in less than 20 cycles. This is also accompanied by the accumulation of residual and irrecoverable strains as shown, for example, in Fig. 10 of this work. Although grain boundaries play a detrimental role in degrading the fatigue properties, relatively inferior fatigue performance was also reported for single crystalline FeMnNiAl [29]. The accumulation of dislocations at the austenite–martensite interface during transformation results in pinning of the boundary thus preventing reverse transformation and in the accumulation of residual martensite. The activation of multiple martensite variants and their interactions with each other and with the coherent nano-scale precipitates also contributes to the pinning of martensite and the subsequent loss of functionality [7]. Under loading conditions where the applied strains are less than the alloy capacity (i.e., transformation occurring in specific locations and not extending across the entire sample), the cyclic degradation is manifested as an accumulation of residual martensite in the initially transforming regions followed by subsequent activation of non-transforming regions. The optical images shown in Fig. 10 represent a clear example of this degrading mechanism. Eventually, the incremental accumulation of plasticity induced residual martensite spreads to cover significant volume of the material leading to complete loss of superelasticity.

The Role of Grain Boundaries

In polycrystalline form, grain boundaries can have a major influence on the accumulation of residual strain and ultimately the nucleation of cracks under fatigue loading. Since martensitic transformation is grain orientation dependent, different interactions between the transformation front/s in one/or both of the grains across the grain boundary can take place. A schematic is shown in Fig. 13 to further illustrate this point. A transformation front can either initiate and move away from the interface or propagate in a manner where it eventually impinges and interacts with the boundary. The interaction between the propagating transformation front and the GB results in high localized stresses in their vicinity. Depending on the crystal orientation across the boundary, subsequent nucleation of transformation in the neighboring, and potentially non-transforming, grain can take place. The fatigue result presented in Fig. 11 of this work is a clear example of this transformation front–GB interaction. It is noted that eventually, the localized deformation in the interaction region resulted in the nucleation of a fatigue crack. It remains unclear how the propensity for nucleating GB cracks would be affected in cases where the relative crystal orientations (i.e., misorientation) would either prevent nucleation in the neighboring grain (complete impedance) or allow transmission of the transformation front across the interface. These cases were not investigated in the current work and literature still lacks a comprehensive study focused on the various types of transformation front–GB interactions and their relative role in inducing GB cracking.

The Effect of Heat Treatment

Significant progress has been made in developing heat treatment condition which promotes good superelasticity in FeMnNiAl SMA. Triggering AGG to produce large-grain material (i.e., bamboo structure) was achieved through high-temperature cycling [15, 30]. The large-grain

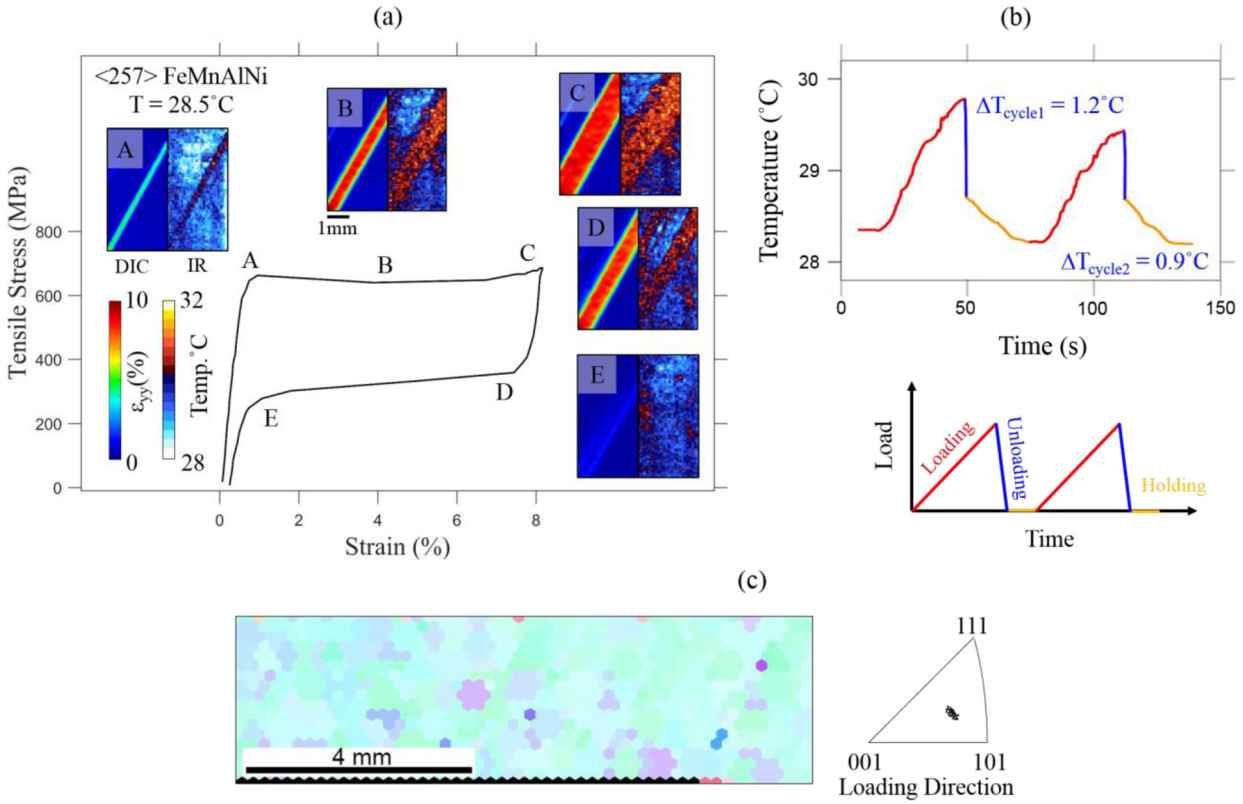

Fig. 12 **a** The superelasticity of a single-crystal FeMnNiAl SMA in tension at 28.5 °C is shown. The temperature, marked as IR in the inset, and strain maps, marked as DIC, are demonstrated side by side in the gauge section. **b** The average temperature data of two consecutive load/unload cycles are plotted against time. The results show that the temperature change upon forward and reverse transformation is less than 2 °C. Such a small variation in temperature has positive attributes in strain rate effects and on fatigue. **c** EBSD mapping of the sample and inverse-pole figure showing the grain orientation of sample (<257>) (Color figure online)

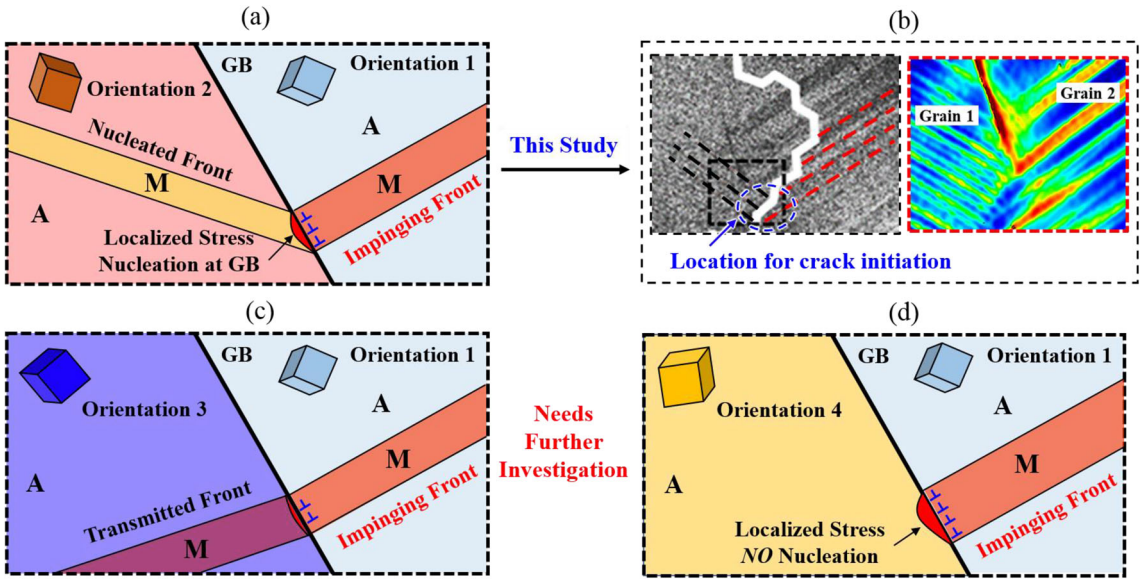

Fig. 13 A schematic showing the interaction between transformation front and grain boundary. **a** A new transformation nucleated from the grain boundary. **b** High-resolution DIC strain contour showing a new transformation front nucleated at the grain boundary. The high strain and stress accumulation at the grain boundary are also conducive to crack initiation. **c** Impinging front transmits into the other grain. **d** No transformation occurs in the other grain after impinging front interacts with the grain boundary. Cases **c** and **d** require further investigation (Color figure online)

bamboo-structure is conducive to superelasticity and reduces the propensity for GB cracking. Following the temperature cycling (typically 900–1200 °C with holding times and multiple cycles), rapid cooling is required to produce a single austenite phase. However, rapid cooling through water quenching has been shown to induce GB cracking even before any application of loading [16]. Quenching into hot 80 °C water eliminates GB cracking. However, fine second phase γ regions (fcc crystal structure) may form in the vicinity of GBs. The presence of this non-transforming second phase has a negative impact on the superelastic properties and fatigue response. In addition to this shortcoming of the current AGG procedures, it should be pointed that although there is control over the resulting grain size, there is no control over the crystal orientation. As the superelastic properties (transformation stress and strain) are grain orientation dependent, e.g., more prone to transformation close to <001>, <148>, and <103> loading directions as shown in Figs. 5 and 9, variation in the achieved properties following AGG is expected. Further dedicated studies are required to address these issues.

In addition to the AGG heat treatment to grow the grains, additional aging treatment is required to create coherent precipitates which can facilitate SE of SMAs and limit the plastic deformation. The most prevalent aging treatment of FeMnNiAl SMA is 200 °C/3 h, where the size of the resultant B2 precipitate is approximately 5–7 nm [30]. Such precipitates have been proven to be beneficial and impart the material with high strength and low stress hysteresis. However, the stability of these precipitates is questionable. A recent study by Ozcan et al. [31] demonstrates that these precipitates will continue to coarsen at room temperature, which significantly alters the mechanical properties, i.e., transformation stress level. The underlying mechanism for this natural aging phenomenon is still a mystery and can potentially become an intriguing topic to study in the future.

Conclusions

The following findings on FeMnNiAl are intriguing and of considerable interest to the community:

(1) The combination of wide superelastic window exceeding 400 °C and low Clausius–Clapeyron slope, 0.5 MPa/°C in tension and 0.18 MPa/°C in compression, is superior to other shape memory alloys.
(2) The transformation stress levels are much higher than most other shape memory alloys. The uniaxial stress levels exceed 500–600 MPa. Such stress levels are achieved in only few SMAs that are more brittle than FeMnNiAl.
(3) The temperature rise during transformation is lower compared to other shape memory alloys which could be beneficial for fatigue resistance under dynamic loading.
(4) The role of grain boundaries is significant. The presence of grain boundaries constitute barriers to transmission of the transformation fronts and could curtail the level of transformation strain and potentially lead to formation of interface cracking.

Acknowledgements The work is supported by Nyquist Chair Funds of University of Illinois. Specimen preparation by FIB and TEM analyses were carried out in the Frederick Seitz Materials Research Laboratory Central Research Facilities, University of Illinois. Financial support by the German Research Foundation (Project No. 250216343 (NI1327/7-3)) and by University of Kassel provided in the framework of the project SmartCon is gratefully acknowledged.

References

1. Hornbogen E, Jost N (1991) Alloys of iron and reversibility of martensitic transformations. Le J Phys IV 1:C4-199–C4-210. https://doi.org/10.1051/jp4:1991430
2. Koval YN, Kokorin VV, Khandros LG (1979) Shape memory effect in Fe-Ni-Co-Ti alloys. Phys Met Met 48:162–164
3. Maki T, Kobayashi K, Minato M, Tamura I (1984) Thermoelastic martensite in an ausaged Fe-Ni-Ti-Co alloy. Scr Metall 18:1105–1109. https://doi.org/10.1016/0036-9748(84)90187-X
4. Sehitoglu H, Karaman I, Zhang X et al (2001) Deformation of FeNiCoTi shape memory single crystals. Scr Mater 44:779–784. https://doi.org/10.1016/S1359-6462(00)00657-6
5. Sehitoglu H, Zhang XY, Kotil T et al (2002) Shape memory behavior of FeNiCoTi single and polycrystals. Metall Mater Trans A 33:3661–3672. https://doi.org/10.1007/s11661-002-0240-0
6. Sehitoglu H, Efstathiou C, Maier HJ, Chumlyakov Y (2005) Magnetization, shape memory and hysteresis behavior of single and polycrystalline FeNiCoTi. J Magn Magn Mater 292:89–99. https://doi.org/10.1016/J.JMMM.2004.10.101
7. Abuzaid W, Sehitoglu H (2018) Superelasticity and functional fatigue of single crystalline FeNiCoAlTi iron-based shape memory alloy. Mater Des 160:642–651. https://doi.org/10.1016/J.MATDES.2018.10.003
8. Chen Q, Andrawes B, Sehitoglu H (2014) Thermomechanical testing of FeNiCoTi shape memory alloy for active confinement of concrete. Smart Mater Struct 23:055015. https://doi.org/10.1088/0964-1726/23/5/055015
9. Kuts OA, Panchenko MY, Kireeva IV, Chumlyakov YI (2015) Shape Memory Effect and Superelasticity in [001] Single Crystals of FeNiCoAlNb(B) Alloys. IOP Conf Ser Mater Sci Eng 93:012034. https://doi.org/10.1088/1757-899X/93/1/012034
10. Chumlyakov YI, Kireeva IV, Kutz OA et al (2016) Unusual reversible twinning modes and giant superelastic strains in FeNiCoAlNb single crystals. Scr Mater 119:43–46. https://doi.org/10.1016/J.SCRIPTAMAT.2016.03.027
11. Omori T, Ando K, Okano M et al (2011) Superelastic effect in polycrystalline ferrous alloys. Science 80(333):68–71. https://doi.org/10.1126/science.1202232

12. Tanaka Y, Himuro Y, Kainuma R et al (2010) Ferrous polycrystalline shape-memory. Science 327(5972):1488–1491
13. Wang J, Sehitoglu H (2014) Dislocation slip and twinning in Ni-based L12 type alloys. Intermetallics 52:20–31. https://doi.org/10.1016/J.INTERMET.2014.03.009
14. Tseng LW, Ma J, Wang SJ et al (2015) Superelastic response of a single crystalline FeMnAlNi shape memory alloy under tension and compression. Acta Mater 89:374–383. https://doi.org/10.1016/J.ACTAMAT.2015.01.009
15. Vollmer M, Krooß P, Kriegel MJ et al (2016) Cyclic degradation in bamboo-like Fe–Mn–Al–Ni shape memory alloys—The role of grain orientation. Scr Mater 114:156–160. https://doi.org/10.1016/J.SCRIPTAMAT.2015.12.007
16. Vollmer M, Segel C, Krooß P et al (2015) On the effect of gamma phase formation on the pseudoelastic performance of polycrystalline Fe–Mn–Al–Ni shape memory alloys. Scr Mater 108:23–26. https://doi.org/10.1016/J.SCRIPTAMAT.2015.06.013
17. Sato A, Chishima E, Soma K, Mori T (1982) Shape memory effect in $\gamma \rightleftarrows \varepsilon$ transformation in Fe-30Mn-1Si alloy single crystals. Acta Metall 30:1177–1183. https://doi.org/10.1016/0001-6160(82)90011-6
18. Watanabe Y, Mori Y, Sato A (1993) Training effect in Fe-Mn-Si shape-memory alloys. J Mater Sci 28:1509–1514. https://doi.org/10.1007/BF00363341
19. Karaca HE, Turabi AS, Chumlyakov YI et al (2016) Superelasticity of [001]-oriented Fe42·6Ni27.9Co17·2Al9.9Nb2.4 ferrous shape memory alloys. Scr Mater 120:54–57. https://doi.org/10.1016/J.SCRIPTAMAT.2016.04.008
20. Ma J, Hornbuckle BC, Karaman I et al (2013) The effect of nanoprecipitates on the superelastic properties of FeNiCoAlTa shape memory alloy single crystals. Acta Mater 61:3445–3455. https://doi.org/10.1016/J.ACTAMAT.2013.02.036
21. Krooß P, Vollmer M, Somsen C, et al (2017) Functional properties of Fe-based shape memory alloys containing finely dispersed precipitates. In: SMAR 2017 - Fourth conference on smart monitoring, assessment and rehabilitation of civil structures. pp 2–9
22. Ojha A, Sehitoglu H (2016) Transformation stress modeling in new Fe-Mn-Al-Ni shape memory alloy. Int J Plast 86:93–111. https://doi.org/10.1016/j.ijplas.2016.08.003
23. Krooß P, Kadletz PM, Somsen C et al (2016) Cyclic degradation of Co49Ni21Ga30 high-temperature shape memory alloy: on the roles of dislocation activity and chemical order. Shap Mem Superelasticity 2:37–49. https://doi.org/10.1007/s40830-015-0049-5
24. Chumlyakov YI, Kireeva IV, Panchenko EY et al (2008) High-temperature superelasticity in CoNiGa, CoNiAl, NiFeGa, and TiNi monocrystals. Russ Phys J 51:1016–1036. https://doi.org/10.1007/s11182-009-9143-5
25. Zhang Y, You Y, Moumni Z et al (2017) Experimental and theoretical investigation of the frequency effect on low cycle fatigue of shape memory alloys. Int J Plast 90:1–30. https://doi.org/10.1016/J.IJPLAS.2016.11.012
26. Nemat-Nasser S, Choi J-Y, Guo W-G, Isaacs JB (2005) Very high strain-rate response of a NiTi shape-memory alloy. Mech Mater 37:287–298. https://doi.org/10.1016/J.MECHMAT.2004.03.007
27. Omori T, Kainuma R (2017) Martensitic transformation and superelasticity in Fe–Mn–Al-based shape memory alloys. Shape Mem Superelasticity 3:322–334. https://doi.org/10.1007/s40830-017-0129-9
28. Vollmer M, Kriegel MJ, Walnsch A et al (2019) On the microstructural and functional stability of Fe-Mn-Al-Ni at ambient and elevated temperatures. Scr Mater 162:442–446. https://doi.org/10.1016/J.SCRIPTAMAT.2018.12.008
29. Vollmer M, Kriegel MJ, Krooß P et al (2017) Cyclic degradation behavior of ⟨001⟩-oriented Fe–Mn–Al–Ni single crystals in tension. Shape Mem Superelasticity 3:335–346. https://doi.org/10.1007/s40830-017-0117-0
30. Ozcan H, Ma J, Wang SJ et al (2017) Effects of cyclic heat treatment and aging on superelasticity in oligocrystalline Fe-Mn-Al-Ni shape memory alloy wires. Scr Mater 134:66–70. https://doi.org/10.1016/j.scriptamat.2017.02.023
31. Ozcan H, Ma J, Karaman I et al (2018) Microstructural design considerations in Fe-Mn-Al-Ni shape memory alloy wires: effects of natural aging. Scr Mater 142:153–157. https://doi.org/10.1016/J.SCRIPTAMAT.2017.07.033